Prospective constraints on the primordial black hole abundance from the stochastic gravitational-wave backgrounds produced by coalescing events and curvature perturbations

Sai Wang,[1,*] Takahiro Terada,[1,†] and Kazunori Kohri[1,2,‡]

[1]*Institute of Particle and Nuclear Studies, KEK, 1-1 Oho, Tsukuba 305-0801, Japan*
[2]*The Graduate University for Advanced Studies (SOKENDAI), 1-1 Oho, Tsukuba 305-0801, Japan*

(Received 29 March 2019; published 28 May 2019; corrected 30 August 2019)

For a variety of ongoing and planned gravitational-wave (GW) experiments, we study expected constraints on the fraction ($f_{\rm PBH}$) of primordial black holes (PBHs) in dark matter by evaluating the energy-density spectra of two kinds of stochastic GW backgrounds. The first one is produced from an incoherent superposition of GWs emitted from coalescences of all of the binary PBHs. The second one is induced through nonlinear mode couplings of large primordial curvature perturbations inevitably associated with the generation of PBHs in the early Universe. In this paper, we focus on PBHs with masses $10^{-8}\ M_\odot \leq M_{\rm PBH} < 1\ M_\odot$, since they are not expected to be of stellar origin. In almost all mass ranges, we show that the experiments are sensitive enough to constrain the fraction for $10^{-5} \lesssim f_{\rm PBH} \lesssim 1$ by considering the GWs from coalescing events and $10^{-13} \lesssim f_{\rm PBH} \lesssim 1$ by considering the GWs from curvature perturbations. Exceptionally, the fraction cannot be constrained for $f_{\rm PBH} \lesssim 10^{-3}$ by these two GW backgrounds only in the narrow mass range around $M_{\rm PBH} \simeq 10^{-7}\ M_\odot$.

DOI: 10.1103/PhysRevD.99.103531

I. INTRODUCTION

The first detection of gravitational waves (GWs) from a binary black hole (BBH) merger by the first Advanced LIGO (aLIGO) observing run [1] has revived extensive interest in primordial black holes (PBHs) [2,3], which are produced directly from the gravitational collapses of the enhanced inhomogeneities in the primordial Universe. The origin of these black holes (BHs) and the formation mechanism of BBHs are still under debate. Besides an astrophysical origin [4–6], the possibility that these BHs are of a primordial origin has also been considered [7–20]. Recently, it has been proposed that the PBHs are capable of accounting for the event rate of BBH mergers observed by aLIGO [7,8], although the formation mechanisms of PBH binaries bring about uncertainties of a couple orders of magnitude (see, e.g., Ref. [20] and references therein). PBHs could be a promising candidate for cold dark matter (CDM) [11]. Currently, the nature of CDM is still uncertain [21]. There is no definitive evidence for weakly interacting massive particles (WIMPs), which are a prime candidate for CDM [22–25]. Conventionally, one defines the abundance of PBHs in CDM as a dimensionless fraction of the form $f_{\rm PBH} = \Omega_{\rm PBH}/\Omega_{\rm CDM}$, where $\Omega_{\rm PBH}$ and $\Omega_{\rm CDM}$ denote the present energy-density fractions of PBHs and CDM, respectively. This quantity has been constrained in a variety of mass ranges by a variety of observations (see, e.g., Refs. [20,26] and references therein), such as the microlensing events caused by massive astrophysical compact halo objects [27–30], the gas accretion effect of PBHs on the cosmic microwave background (CMB) [31–33], the null detection of a third-order Shapiro time delay using a pulsar-timing array [34], and the claimed event rate of BBH mergers from aLIGO [7,8,35].

PBHs can be also a useful probe of the primordial curvature perturbations [36], since the former are formed via the direct gravitational collapse of the latter [2,3]. Contrary to the astrophysical processes for which only BHs heavier than $\mathcal{O}(1)$ solar mass can be produced [37], small-mass BHs could also be produced by the strong gravity inside the highly compressed overdensities in the early Universe [38]. The PBH mass depends on the PBH formation redshift z_f, namely, $M \simeq 30\,M_\odot[4\times10^{11}/(1+z_f)]^2$ [8], where $M_\odot$ is the solar mass ($= 2\times10^{33}$ g). Since inflation models [39–45] predict the properties of the primordial curvature perturbations, which determine the mass and abundance of PBHs (see, e.g., Refs. [20,26,46–48] and references therein), our observational knowledge of PBHs is important to learn about the physics of the inflationary Universe.

Recently, it has been proposed that the energy-density fraction of PBHs can be constrained by measuring the energy-density spectrum of the stochastic gravitational-wave background (SGWB). First, the SGWB can be

*wangsai@post.kek.jp
†teradat@post.kek.jp
‡kohri@post.kek.jp

produced from an incoherent superposition of GWs emitted from all of the coalescing PBH binaries. The null detection of such a SGWB by the first aLIGO observing run [49] has been used to independently constrain $f_{\rm PBH}$ [50–53]. For example, Ref. [50] obtained the tightest observational constraint on $f_{\rm PBH}$ in the mass range 1–$10^2\ M_\odot$, improving the existing observational constraints by 1 order of magnitude. The possibility to detect the SGWB from PBHs (in particular, from subsolar-mass PBHs) by upcoming aLIGO observing runs was also predicted [50]. Second, the SGWB is induced from the enhanced primordial curvature perturbations [54–57].[1] By making use of the semianalytic calculation of the induced GW spectrum [76,77], the null detection of such a SGWB by a variety of GW detectors has been used to obtain constraints on the spectral amplitude of primordial curvature perturbations [78–80]. The constraints on the induced SGWB can be recast as the constraints on the abundance of PBHs, and vice versa [69,81–84].

In this paper, we focus on small-mass PBHs with $10^{-8}\ M_\odot \leq M_{\rm PBH} \leq 1\ M_\odot$. Correspondingly, we calculate the energy-density fraction of the above two kinds of SGWBs, and report the expected constraints on the energy-density fraction of PBHs from the null detection of the SGWBs by several ongoing and planned GW experiments (see details in Ref. [85]), which include the Square Kilometre Array (SKA) [86], Laser Interferometer Space Antenna (LISA) [87,88], DECi-hertz Interferometer Gravitational wave Observatory (DECIGO) [89] and B-DECIGO [90], Big Bang Observer (BBO) [91], Einstein Telescope (ET) [92], and aLIGO [93]. Although we focus on the mass range $10^{-8}\ M_\odot \leq M_{\rm PBH} \leq 1\ M_\odot$, the method of our analysis is equally applicable to PBH masses outside of this range. In this context, the authors of Refs. [94,95] studied the SGWB induced by the curvature perturbations associated with PBHs with masses around $10^{-12}\ M_\odot$ as it may explain the whole abundance of the dark matter. The authors of Ref. [79] obtained constraints on the primordial curvature perturbations by studying the detectability of the curvature-induced SGWB in a wide frequency range corresponding to a wide PBH mass range.

First, following Ref. [50], we evaluate the energy-density fraction of the SGWB from binary PBH coalescence, by assuming a monochromatic mass distribution of PBHs. This choice of the delta function is reasonable since the mass distribution of PBHs is insensitive to the details of the spectral shape of primordial curvature perturbations, especially after taking into account coarse graining within the Hubble horizon and the effects of critical collapse [47]. In addition, the inflation scenario does not favor a significantly extended PBH mass distribution [11]. Second, following Ref. [76], we evaluate the energy-density fraction of the induced SGWB by assuming a delta function for the power spectrum of primordial curvature perturbations. In principle, the spectrum of the induced SGWB depends on the details of the spectral shape of primordial curvature perturbations. Recently, Ref. [79] found a spread of the SGWB spectrum by studying a log-normal distribution for the power spectrum of primordial curvature perturbations. So the results obtained in our paper can be regarded as conservative.[2] See also Ref. [96] which discussed the effects of a broad spectrum.

The rest of the paper is arranged as follows. In Sec. II, we briefly review the formation of PBHs in the early Universe, given the power spectrum of primordial curvature perturbations. In Sec. III, we evaluate the energy-density fraction of the SGWB from binary PBH coalescence, and use it to obtain expected constraints on $f_{\rm PBH}$ from a variety of ongoing and planned GW detectors. In Sec. IV, we evaluate the induced SGWB from the enhanced primordial curvature perturbations, and obtain the expected constraints on the energy-density fraction of PBHs from SKA and LISA. The conclusions and discussions are given in Sec. V.

II. FORMATION OF PRIMORDIAL BLACK HOLES

Given the power spectrum of primordial curvature perturbations, we can evaluate the probability of PBH production, the mass function of PBHs, and the PBH abundance [20,26]. In this work we assume that PBHs are formed in the early Universe which is radiation dominated (RD). First of all, we need to estimate the wave-number scale k which is related to a given mass scale M_H within the Hubble horizon at the time of horizon reentry. According to the Appendix A, it is represented by

$$\frac{k}{k_*} = 7.49 \times 10^7 \left(\frac{M_\odot}{M_H}\right)^{1/2} \left(\frac{g_{*,\rho}(T(M_H))}{106.75}\right)^{1/4} \times \left(\frac{g_{*,s}(T(M_H))}{106.75}\right)^{-1/3}, \tag{1}$$

where $k_* = 0.05\ {\rm Mpc}^{-1}$. Here we can numerically obtain the temperature at formation $T(M_H)$ by using Eq. (A6). The effective degrees of freedom of relativistic particles, i.e., $g_{*\rho}$ and g_{*s}, were precisely calculated for the Standard

[1] Based on the inflation model, primordial GWs [39,58] are decoupled from primordial curvature perturbations at the first order. However, the induced GWs can be generated from primordial curvature perturbations at the second order. Whether or not primordial GWs are detected in the future [59–68], the induced GWs could be sizable and may even be larger than primordial GWs if the primordial curvature perturbations are significantly enhanced [54–56,69–75].

[2] This is not that simple because the spectral index of the tails of the SGWB is also relevant as well as the width around the peak, and the spectral index depends on the shape of the curvature perturbations. See the discussion around Eq. (58) of Ref. [77]. Anyway, we focus on the delta function case for definiteness.

Model in Ref. [97]. Here we interpolate the tabulated data provided at the website[3] associated with this reference.

The phenomena of critical collapse [11,98] could describe the formation of PBHs with mass M in the early Universe, depending on the horizon mass M_H and the amplitude of density fluctuations δ. We have the following relation:

$$M = KM_H(\delta - \delta_c)^\gamma, \tag{2}$$

where $K = 3.3$, $\gamma = 0.36$, and $\delta_c = 0.45$ are numerical constants.[4] The above equation can be inverted to express δ in terms of M/M_H, namely, $\delta = (M/(KM_H))^{1/\gamma} + \delta_c$, which is useful in the following calculations.

In the RD Universe, the coarse-grained density perturbation is given by

$$\sigma^2(k) = \int_{-\infty}^{+\infty} d\ln q\, w^2(q/k)\left(\frac{4}{9}\right)^2\left(\frac{q}{k}\right)^4 \times T^2(q, \tau = 1/k)P_\zeta(q), \tag{3}$$

where $w(q/k) = \exp(-q^2/(2k^2))$ is a Gaussian window function, and $T(q,\tau) = 3(\sin y - y\cos y)/y^3$ ($y \equiv q\tau/\sqrt{3}$) is a transfer function (see, e.g., Refs. [101,102] for details). We consider the power spectrum of primordial curvature perturbations $P_\zeta(k)$ to be a delta function of $\ln k$, i.e.,

$$P_\zeta(k) = A\delta(\ln k - \ln k_0), \tag{4}$$

where k_0 is a given constant wave number, and A is a dimensionless amplitude. By substituting Eq. (4) into Eq. (3), we obtain

$$\sigma^2(k) = 16Ae^{-1/x^2}\left[\cos^2\left(\frac{1}{\sqrt{3}x}\right) + x\left(3x\sin^2\left(\frac{1}{\sqrt{3}x}\right) - \sqrt{3}\sin\left(\frac{2}{\sqrt{3}x}\right)\right)\right], \tag{5}$$

where $x \equiv k/k_0$ is a dimensionless quantity. We show $\sigma^2(k)/A$ versus k/k_0 in Fig. 8 at the end of Appendix A.

To convert $\sigma(k)$ to the mass function of PBHs, by making use of the Press-Schechter formalism [103] we calculate the probability of PBH production, i.e.,

$$\beta_{M_H} = \int_{\delta_c}^{\infty}\frac{M}{M_H}\mathcal{P}_{M_H}(\delta(M))d\delta(M) = \int_{-\infty}^{\infty}\frac{M}{M_H}\mathcal{P}_{M_H}(\delta(M))\frac{d\delta(M)}{d\ln M}d\ln M \equiv \int_{-\infty}^{\infty}\tilde{\beta}_{M_H}(M)d\ln M, \tag{6}$$

which accounts for the fraction of the Hubble volumes that collapse into PBHs when the horizon mass is M_H. $\tilde{\beta}_{M_H}(M)$ is the distribution of the (logarithmic) masses of PBHs resulting after the critical collapse. Here $\mathcal{P}_{M_H}(\delta)$ denotes a Gaussian probability distribution of primordial density perturbations at the given horizon scale corresponding to M_H. It is represented by

$$\mathcal{P}_{M_H}(\delta(M)) = \frac{1}{\sqrt{2\pi\sigma^2(k(M_H))}}\exp\left(-\frac{\delta^2(M)}{2\sigma^2(k(M_H))}\right), \tag{7}$$

where $\sigma(k(M_H))$ is computed by making use of Eq. (5), and $k(M_H)$ is given by Eq. (1). The explicit form of $\tilde{\beta}_{M_H}(M)$ is [104]

$$\tilde{\beta}_{M_H}(M) = \frac{K}{\sqrt{2\pi}\gamma\sigma(k(M_H))}\left(\frac{M}{KM_H}\right)^{1+\frac{1}{\gamma}} \times \exp\left(-\frac{1}{2\sigma^2(k(M_H))}\left(\delta_c + \left(\frac{M}{KM_H}\right)^{\frac{1}{\gamma}}\right)^2\right). \tag{8}$$

The mass function of PBHs is defined as $f(M) = \frac{1}{\Omega_{\rm CDM}}\frac{d\Omega_{\rm PBH}}{d\ln M}$, and the abundance of PBHs in CDM is given by $f_{\rm PBH} = \int f(M)\mathrm{d}\ln(M/M_\odot)$. We obtain the mass function of PBHs as follows (see, e.g., Ref. [47]):

$$f(M) = \frac{\Omega_{\rm m}}{\Omega_{\rm CDM}}\int_{-\infty}^{\infty}\left(\frac{g_{*,\rho}(T(M_H))}{g_{*,\rho}(T_{\rm eq})}\frac{g_{*,s}(T_{\rm eq})}{g_{*,s}(T(M_H))}\frac{T(M_H)}{T_{\rm eq}}\right) \times \tilde{\beta}_{M_H}(M)d\ln M_H, \tag{9}$$

where $T_{\rm eq}$ is the temperature of the Universe at the epoch of matter-radiation equality. In Fig. 1, we depict several examples (colored solid curves) for the mass function $f(M)$ which is originated from $P_\zeta(k)$ in Eq. (4). To be specific, we choose the horizon mass to be $M_H = 10^{-i}M_\odot (i = 0, 1, 2, \ldots, 8)$, each of which determines the value of its own $k_0 = k_0(M_H)$. Here (10^2A) is 5.8898, 5.4658, 5.1116, 4.8011, 4.6799, 4.6490, 4.3002, 3.8740, and 3.6813, respectively, so that $f_{\rm PBH}$ equals the upper limit on $f(M)$ with the aforementioned values of M_H. For comparison, we plot the existing observational constraint (red dashed curve) on the PBH mass function. The constraint used here arises from the microlensing

[3] http://member.ipmu.jp/satoshi.shirai/EOS2018.

[4] Analytically, it is estimated to be $\delta_c = 0.41$ [99]. In fact, however, they depend on the radial profile of the density perturbations. [100]

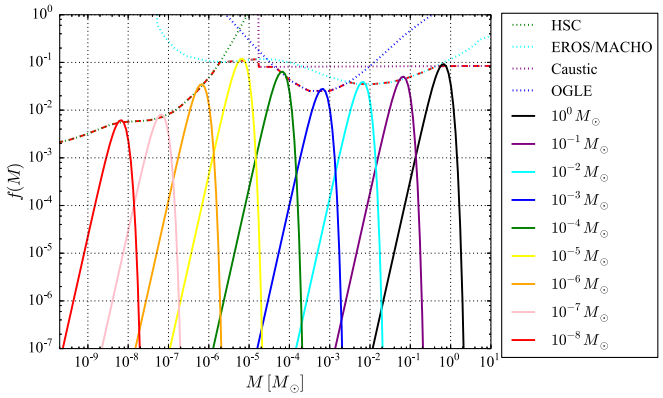

FIG. 1. Mass functions $f(M)$ originated from the delta function power spectrum $P_\zeta(k)$ (colored solid curves). From right to left, based on Eq. (1), the value of k_0 is chosen so that the corresponding M_H is $\log_{10}(M_H/M_\odot) = 0, -1, -2, -3, -4, -5, -6, -7, -8$. The normalization A is chosen so that $f_{\rm PBH}$ is equal to the upper bound on $f(M)$ with the aforementioned values of M_H. To be specific, we take 10^2A as 5.8898, 5.4658, 5.1116, 4.8011, 4.6799, 4.6490, 4.3002, 3.8740, and 3.6813, respectively. The existing observational constraints [HSC [105] (green dotted), OGLE [106] (blue dotted), EROS/MACHO [107,108] (cyan dotted), caustic crossing [109] (purple dotted), and their combination (red dashed)] are plotted for comparison.

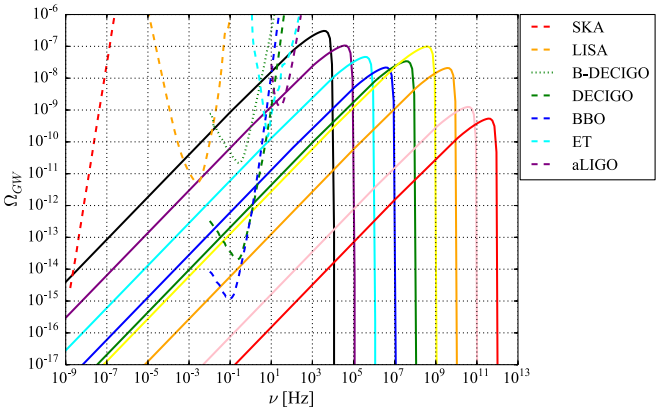

FIG. 2. Energy-density spectrum (colored solid curves) of the SGWB due to binary PBH coalescence which is just allowed by the existing observational constraints on the PBH abundance. The SGWB spectra with the cutoff frequencies from right to left correspond to the peaks from left to right in Fig. 1 (same colors). The sensitivity curves (colored dashed/dotted) of the GW detectors are also plotted for comparison.

observations of Subaru/HSC [105], OGLE [106], EROS-2 [107], MACHO [108], and the caustic crossing [109].

III. STOCHASTIC GRAVITATIONAL-WAVE BACKGROUND DUE TO BINARY PRIMORDIAL BLACK HOLE MERGERS

Two different mechanisms have been proposed to form binaries from PBHs. One scenario assumes that two PBHs could form a binary due to the energy loss via gravitational radiation when they pass by each other accidentally in the late Universe [7,9]. The other one assumes that two nearby PBHs form a binary due to the tidal force from a third neighboring PBH in the early Universe [8,110,111]. Both scenarios are capable of explaining the merger rates of BBHs reported by aLIGO. However, the first one requires the PBHs to contribute most of the CDM, which is disfavored by various observational constraints in the relevant mass range. On the other hand, the second one is still allowed. In this work, we thus adopt the formation scenario[5] of PBH binaries proposed in Ref. [110] and revisited by Refs. [8,10,35,111–118]. In Appendix B we give a brief summary of the formalism for such a scenario.

We calculate the SGWB spectrum produced from the coalescing PBH binaries. In general, the dimensionless energy-density spectrum of the SGWB is defined as $\Omega_{\rm GW} = \rho_{\rm c}^{-1} d\rho_{\rm GW}/d\ln\nu$, where $\rho_{\rm GW}$ is the GW energy density and ν is the GW frequency [119]. Knowing the merger rate of PBH binaries in Eq. (B2), according to Ref. [50], we can compute the SGWB energy-density spectrum within the frequency interval $(\nu,\ \nu + d\nu)$. It is given by

$$\Omega_{\rm GW}(\nu) = \frac{\nu}{\rho_{\rm c}} \int_0^{\frac{\nu_{\rm cut}}{\nu}-1} \frac{R_{\rm PBH}(z)}{(1+z)H(z)} \frac{dE_{\rm GW}}{d\nu_{\rm s}}(\nu_{\rm s}) dz, \qquad (10)$$

where $\frac{dE_{\rm GW}}{d\nu_{\rm s}}(\nu_{\rm s})$ is the GW energy spectrum of a BBH coalescence (see details in Refs. [120,121], or a brief summary in Appendix C), $\nu_{\rm s}$ is the frequency in the source frame and is related to the observed frequency ν through $\nu_{\rm s} = (1+z)\nu$, and $\nu_{\rm cut}$ is the cutoff frequency for a given BBH system.

For PBH binaries with component masses $10^{-i}M_\odot (i = 0, 1, 2, \ldots, 8)$, which correspond to the examples of the PBH mass function in Fig. 1, we plot the corresponding energy-density fractions of the SGWB due to binary PBH coalescence at the existing observational constraints on the PBH abundance in Fig. 2. The color coding is the same as that in Fig. 1. For comparison, we depict the sensitivity curves[6] of several GW experiments (colored dashed/dotted curves), which include a pulsar-timing array (SKA [86]), space-based GW interferometers (LISA [88], DECIGO [89] and B-DECIGO [90], BBO [91]), a third-generation

[5]In this section, we use the revised formalism in Ref. [20], instead of the original one in Ref. [8].

[6]Sometimes, only the amplitude spectral density $S_n(f)$ is shown for a given gravitational-wave detector. We have $\sqrt{S_n(f)} = h_n(f) f^{-1/2}$, which has units of $\mathrm{Hz}^{-1/2}$, and h_n is the noise amplitude. The sensitivity to the SGWB energy density is related to $S_n(f)$ by $\Omega_{\mathrm{GW},n}(f) = 3.132 \times 10^{35} h^{-2} (f/\mathrm{Hz})^3 \times (\sqrt{S_n(f)}/\mathrm{Hz}^{-1/2})^2$ [122,123]. The reduced Hubble constant is $h = 0.678$ in this paper.

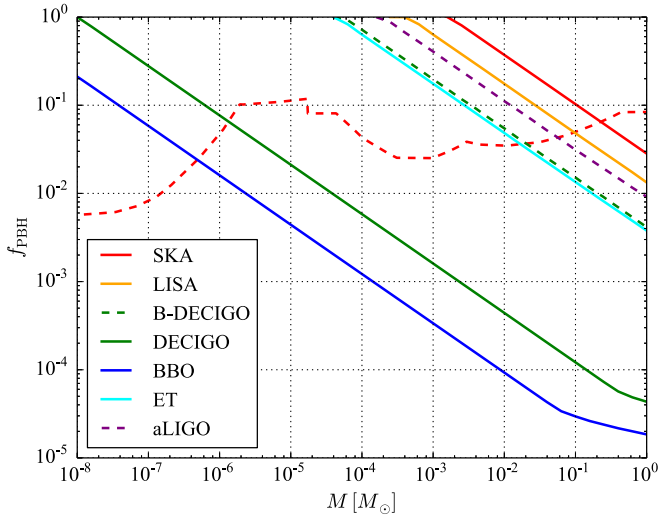

FIG. 3. Expected constraints on the PBH abundance from the null detection of the SGWB by LISA (orange solid), B-DECIGO (green dashed), DECIGO (green solid), BBO (blue solid), ET (cyan solid), and aLIGO (purple dashed). The present existing constraint (red dashed) is plotted for comparison.

ground-based GW interferometer (ET [92]), and a second-generation ground-based GW interferometer (aLIGO [93]). If the spectrum predicted in a model intersects the sensitivity curve of a given experiment, the expected signal-to-noise ratio is equal to or greater than unity, which implies a possible detection of such a spectrum by this experiment.

Null detection of the SGWB by a given future or ongoing GW experiment can place an upper bound on the magnitude of the energy-density fraction of the SGWB in a given frequency band, and can be further recast to constrain the maximum PBH abundance. From Fig. 2, we see that all of the GW experiments could potentially contribute to the improvement of existing observational constraints on the PBH abundance, since their sensitivity curves intersect some spectra. Therefore, by regarding the sensitivity curves of all of these experiments as upper bounds on the SGWB spectrum, we evaluate the expected upper limits on the PBH abundance from these experiments. We depict our results in Fig. 3.

Our results are as follows. SKA, LISA, and aLIGO will give us relatively weak constraints in the future. It is notable that this expected limit from aLIGO is surely stronger than the current one, which was reported recently in Ref. [35]. Both ET and B-DECIGO also have similar constraints on the abundance. All four of the above experiments are expected to improve the existing observational constraints on the subsolar-mass PBHs. However, both DECIGO and BBO are expected to significantly improve the existing constraints over the mass range $\mathcal{O}(10^{-6}) \leq M/M_\odot \leq \mathcal{O}(10^{0})$.

IV. STOCHASTIC GRAVITATIONAL-WAVE BACKGROUND INDUCED BY PRIMORDIAL CURVATURE PERTURBATIONS

The SGWB can be also induced by enhanced primordial curvature perturbations via the scalar-tensor mode coupling in the second-order perturbation theory [55]. In Appendix D, we give a brief summary of the evaluation of the induced SGWB spectrum. For details, see Ref. [76] and references therein. In the following, we will use the formulas summarized in Appendix D to calculate the energy-density spectrum of the induced SGWB, given the form of $P_\zeta(k)$ in Eq. (4). We consider the minimal case in which the statistics of the curvature perturbations is Gaussian[7] and neglect the time evolution of the mass function of PBHs due to accretion, but generalizations can be found in Ref. [127].

According to Eqs. (D1)–(D3), we obtain the dimensionless energy-density spectrum of the induced SGWB as

$$\Omega_{\rm IGW}\left(\nu=\frac{k}{2\pi}\right)=\Omega_{\rm r,0}\left(\frac{g_*(T(k))}{g_*(T_{\rm eq})}\right)\left(\frac{g_{*,s}(T(k))}{g_{*,s}(T_{\rm eq})}\right)^{-4/3}\times\frac{3A^2}{64}\left(\frac{4-\tilde{k}^2}{4}\right)^2\tilde{k}^2(3\tilde{k}^2-2)^2$$
$$\times\left[\pi^2(3\tilde{k}^2-2)^2\Theta(2-\sqrt{3}\tilde{k})+\left(4+(3\tilde{k}^2-2)\ln\left|1-\frac{4}{3\tilde{k}^2}\right|\right)^2\right]\Theta(2-\tilde{k}),\tag{11}$$

where $\nu=k/2\pi$ denotes the frequency of GWs, and the dimensionless wave number $\tilde{k}=k/k_0$ is introduced for simplicity. Based on Appendix A, the cosmic temperature T can be numerically related to M_H and k, and then to ν. Here, $\Theta(x)$ denotes the Heaviside theta function with variable x.

Similarly to Fig. 2, we plot the energy-density fractions of the induced SGWB due to the enhanced primordial curvature perturbations in Fig. 4. Both A and k_0 are chosen as those in Sec. II. The same color coding is used as in Fig. 1. The double-peak structures

[7]The statistical properties of curvature perturbations can modify the relation between the amount of induced SGWB and the PBH abundance. Even if the curvature perturbations are completely Gaussian, the density contrasts are non-Gaussian due to the nonlinear nature of gravity, as shown recently in Refs. [48,124–126].

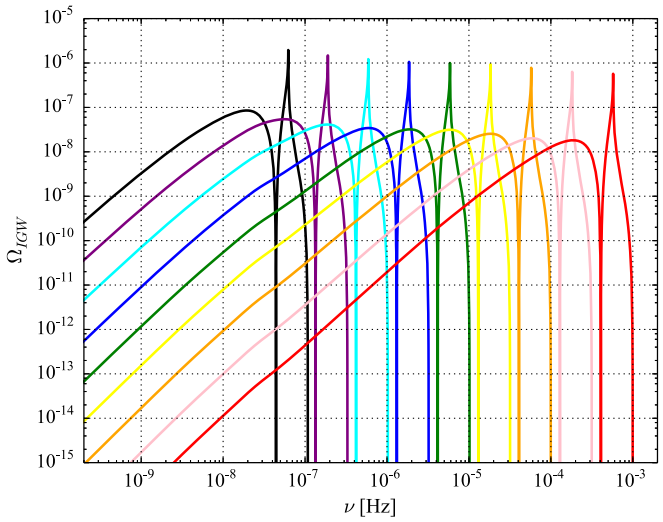

FIG. 4. Energy-density spectrum of the SGWB nonlinearly induced by primordial curvature perturbations. The SGWB spectra (colored solid curves) with peaks from right to left correspond to the mass functions with peaks from left to right in Fig. 1 (same colors).

arise from the fact that $P_\zeta(k)$ is assumed to be a delta function [Eq. (4)]. For a broader distribution for $P_\zeta(k)$ (e.g., the log-normal distribution in Ref. [79]), one could find the spread of the SGWB spectrum. Therefore, our discussions in the next two paragraphs could be regarded as conservative.

In Fig. 5, besides the energy-density spectra of the induced SGWB (colored solid curves, same as in Fig. 4), we depict the sensitivity curves of SKA [86] (red dashed) and LISA [88] (orange dashed) for comparison. For a given spectrum of the induced SGWB, we conservatively drop the right-handed peak since such a spiky structure exists only for source spectra with tiny widths. Similarly to the discussions in the last section, if a model-predicting spectrum intersects the sensitivity curve of a given experiment, it is possible to measure such a spectrum with this experiment. In such a case, both SKA and LISA are expected to exclude most of the parameter space, or equivalently improve the existing observational constraints on the PBH abundance significantly.

Assuming the null detection of the induced SGWB from enhanced primordial curvature perturbations, similarly to Fig. 3, we plot the expected constraints on the PBH abundance from SKA (red shaded) and LISA (orange shaded) in Fig. 6. The shaded regions represent the parts of the parameter space that are excluded by these experiments. In fact, here we first obtain the constraints on A from the induced SGWB, and then recast them as the upper limits on $f_{\rm PBH}$ according to the formulas in Sec. II.

Finally, we can combine the results in Fig. 3 with Fig. 6 to obtain Fig. 7. Generally speaking, the slopes of the upper bounds (i.e., boundaries of shaded regions) from the induced SGWB are significantly sharper than those (i.e., colored curves) from the SGWB due to coalescing PBH binaries. This property can be easily understood as follows. On the one hand, we directly constrained the magnitude of $f_{\rm PBH}$ by calculating the SGWB from coalescing PBH binaries. The detection of such a SGWB requires a significant amount of PBH binaries in the Universe. This implies that the GW detectors can probe enhanced primordial curvature perturbations only if $A \sim \mathcal{O}(0.1)$. When $A \ll \mathcal{O}(0.1)$, there would be so few PBHs in the Universe that the thresholds of GW detectors would not be triggered.

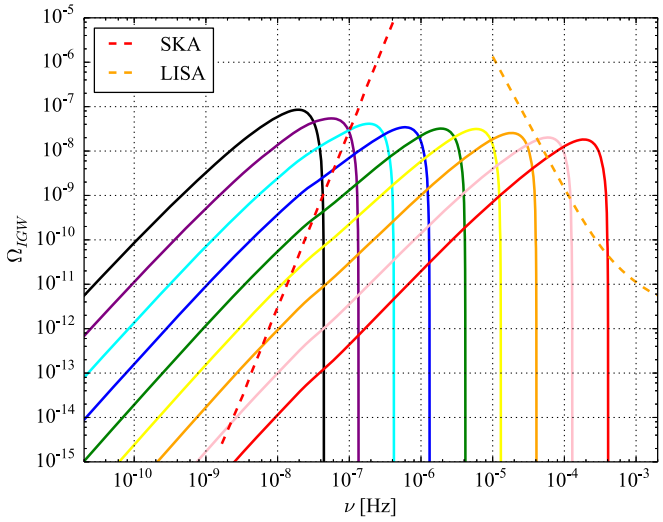

FIG. 5. Similarly to Fig. 4, we plot the energy-density spectrum of the induced SGWB (colored solid curves), but the right-handed peak is conservatively dropped. We depict the sensitivity curves of SKA (red dashed) and LISA (orange dashed) for comparison.

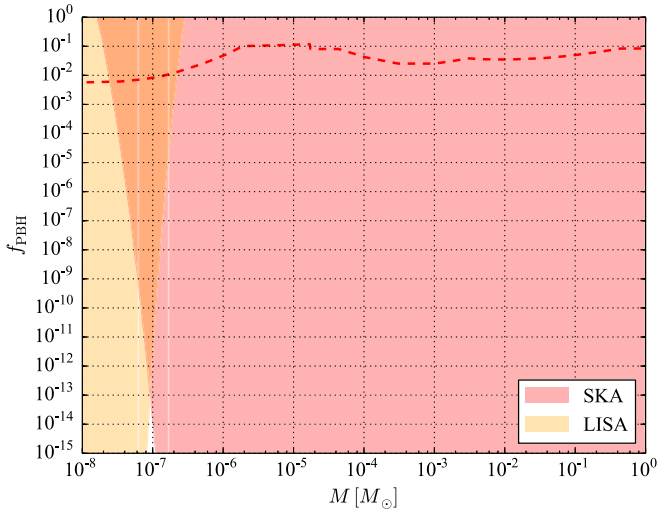

FIG. 6. Expected constraints on the PBH abundance versus the PBH mass from the null detection of the induced SGWB by SKA (red shaded) and LISA (orange shaded). The existing observational constraint (red dashed) is also plotted for comparison.

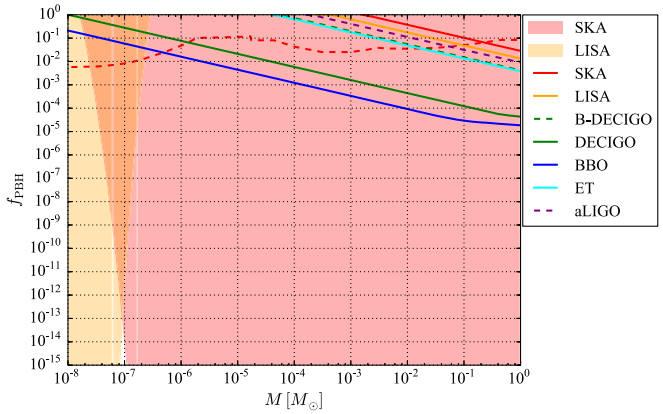

FIG. 7. Expected constraints on the PBH abundance versus the PBH mass from the null detection of the two kinds of SGWBs. The existing observational constraint (red dashed) is plotted for comparison.

On the other hand, by detecting the induced SGWB, we directly obtained the constraints on A, which were recast as the indirect constraints on $f_{\rm PBH}$. In fact, by detecting the induced SGWB, the GW detectors can probe the primordial curvature perturbations of arbitrary amplitudes within their sensitivities. Since the induced SGWB spectrum is proportional to A^2 while $f_{\rm PBH}$ is exponentially sensitive to A, we obtained sharper slopes for the upper bounds from the induced SGWB than those from the SGWB due to coalescing PBH binaries in Fig. 7. Thus, the constraints on $f_{\rm PBH}$ from the SGWB induced by curvature perturbations are stronger than those from the SGWB whose origin is merger events, except for a narrow gap around $10^{-7}\ M_\odot$ corresponding to the relatively weak observational sensitivity around about 10^{-6} Hz. Nevertheless, both types of SGWB are complementary and useful as a consistency check of the PBH hypothesis since these two types of SGWB have their own individual features in the spectra and are probed by different observations which are supposed to measure GWs at different frequency bands.

V. CONCLUSIONS

It has been known that PBHs can form binaries in the early Universe, and a PBH binary can merge into a new heavier BH due to the energy loss via gravitational radiation. Based on Ref. [8], the merger rate of PBH binaries depends on the abundance and mass of PBHs. Given the existing constraints on the mass function of PBHs, following Ref. [50], we have evaluated the energy-density spectra of SGWBs which arise from coalescences of PBH binaries with component masses $10^{-i}\ M_\odot (i = 0, 1, 2, \ldots, 8)$. From Fig. 2, we found that some of them intersect the sensitivity curves of several future GW experiments. This means that the existing limits can be improved by these experiments in the future if these experiments do not detect the SGWB. By making use of these sensitivity curves as upper limits on the SGWB energy-density fraction, we have evaluated the expected upper limits on the abundance of PBHs, and shown our results in Fig. 3. In particular, both DECIGO and BBO are expected to significantly improve the existing limits over the mass range $10^{-6}\ M_\odot$–$10^{0}\ M_\odot$.

The generation of PBHs in the early Universe requires large amplitudes of the primordial curvature perturbations, which can always induce the SGWB. By taking into account the existing constraints on the mass function of PBHs and making use of the semianalytic formula in Ref. [76], we have calculated the energy-density spectrum of the induced SGWB, and shown our results in Fig. 4. We found several intersections between the induced SGWB spectra and the sensitivity curves of SKA and LISA in Fig. 5. This implies that these experiments can improve the existing upper limits on the mass function of PBHs in the future if they claim a null detection of the induced SGWB energy-density fraction. In this case, the shaded regions in Fig. 6 will be excluded by SKA and LISA, respectively.

Finally, by combining Fig. 3 with Fig. 6 to obtain Fig. 7, we found stronger constraints on $f_{\rm PBH}$ from the SGWB induced by curvature perturbations than those from the SGWB due to coalescing events, except for a narrow gap around $10^{-7}\ M_\odot$. However, both types of SGWB are complementary and useful as a consistency check of the PBH hypothesis.

ACKNOWLEDGMENTS

This work is supported in part by the JSPS Research Fellowship for Young Scientists (T. T.) and JSPS KAKENHI Grants No. JP17H01131 (S. W. and K. K.) and No. JP17J00731 (T. T.), and MEXT KAKENHI Grants No. JP15H05889 (K. K.), and No. JP18H04594 (K. K.).

APPENDIX A: RELATION BETWEEN k AND M_H IN THE RADIATION DOMINATED UNIVERSE

During the RD era of the Universe, the relation between the wave number k and the horizon mass M_H is obtained as follows. By definition, we have

$$k = a(M_H)H(M_H). \tag{A1}$$

The value of the scale factor $a(M_H)$, when the mode corresponding to M_H reenters the Hubble horizon, is obtained by using entropy conservation,

$$\frac{a(M_H)}{a_0(=1)} = \left(\frac{g_{*,s}(T_0)}{g_{*,s}(T(M_H))}\right)^{1/3} \frac{T_0}{T(M_H)}, \tag{A2}$$

where $T_0 = 2.725$ K denotes the present temperature of the CMB, and the temperature $T(M_H)$ is given by the Friedmann equation, i.e.,

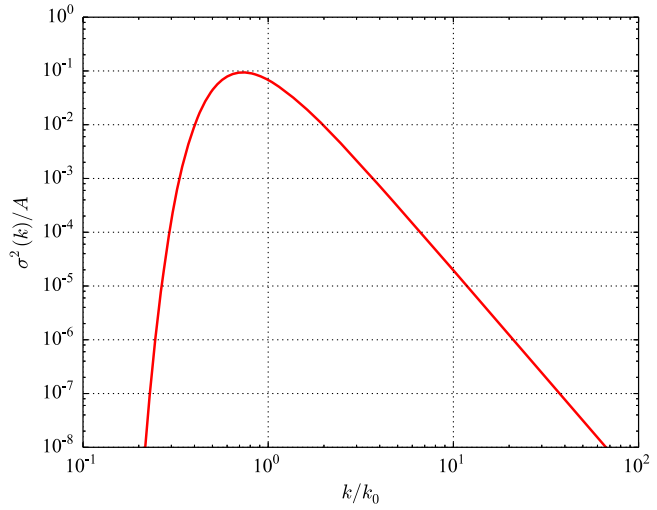

FIG. 8. Coarse-grained density function calculated by assuming that $P_\zeta(k)$ is a delta function of $\ln k$.

$$3H^2(M_H)M_{\rm G}^2 = \rho \approx \rho_{\rm rad} = \frac{\pi^2 g_{*,\rho}(T(M_H))}{30} T^4(M_H), \tag{A3}$$

where $M_{\rm G} = M_{\rm P}/\sqrt{8\pi}$ is the reduced Planck mass. The relation between the horizon mass M_H and the Hubble radius H^{-1} is given by

$$M_H = \frac{4\pi}{3}(H(M_H))^{-3}\rho. \tag{A4}$$

Combining Eq. (A4) with the left equality of Eq. (A3), we have the following formula between H and M_H:

$$H(M_H) = 4\pi \frac{M_{\rm G}^2}{M_H}. \tag{A5}$$

By combining Eq. (A5) with the right equality of Eq. (A3), we thus obtain a relation between M_H and T, i.e.,

$$M_H = 12\left(\frac{10}{g_{*,\rho}(T)}\right)^{1/2} \frac{M_G^3}{T^2}. \tag{A6}$$

Combining Eqs. (A1), (A2), (A5), and (A6), we obtain

$$\frac{k}{k_*} = 7.49 \times 10^7 \left(\frac{M_\odot}{M_H}\right)^{1/2} \left(\frac{g_{*,\rho}(T(M_H))}{106.75}\right)^{1/4} \times \left(\frac{g_{*,s}(T(M_H))}{106.75}\right)^{-1/3}, \tag{A7}$$

where $M_\odot$ denotes the solar mass and $k_* = 0.05\ {\rm Mpc}^{-1}$.

In Fig. 8 we show $\sigma^2(k)/A$ versus k/k_0. In wave-number space, the peak of the coarse-grained perturbations shifts from the original peak k_0. Numerically, the shifted peak is obtained as $k = 0.730715 k_0$,

$$\frac{k_{(\text{peak of PBHs})}}{k_{(\text{peak of primordial curvature perturbations})}} = 0.730715. \tag{A8}$$

In our example, by assuming that $P_\zeta(k)$ is a delta function, the wave number in the denominator is nothing but k_0. When a PBH forms, the shorter scales have already experienced the radiation pressure and have been smoothened. Therefore, the PBH mass scale corresponds to the coarse-grained perturbation scale. In other words, k in Eqs. (1) and (A7) should be the one appearing in the numerator of the left-hand side of Eq. (A8).

APPENDIX B: FORMALISM FOR THE MERGER RATE OF PBH BINARIES

Given the fraction of PBHs in CDM (namely, $f_{\rm PBH}$[8]) for a fixed PBH mass M, the probability that a PBH binary coalesces within the cosmic time interval $(t, t+dt)$ is given by (see, e.g., Refs. [8,20] for details)

$$dP_t = \begin{cases} \frac{3}{58}\left[-\left(\frac{t}{t_0}\right)^{\frac{3}{8}} + \left(\frac{t}{t_0}\right)^{\frac{3}{37}}\right]\frac{dt}{t} & \text{for } t < t_c, \\ \frac{3}{58}\left(\frac{t}{t_0}\right)^{\frac{3}{8}}\left[-1 + \left(\frac{t}{t_c}\right)^{-\frac{29}{56}}\left(\frac{4\pi}{3} f_{\rm PBH}\right)^{-\frac{29}{8}}\right]\frac{dt}{t} & \text{for } t \geq t_c, \end{cases} \tag{B1}$$

where we define $t_0 = (3/170)\{\bar{x}^4/[(GM)^3(4\pi f_{\rm PBH}/3)^4]\}$ and $t_c = t_0(4\pi f_{\rm PBH}/3)^{37/3}$, and $\bar{x} = [3M/(4\pi\rho_{\rm PBH,eq})]^{1/3}$ is the physical mean separation of PBHs at the epoch of matter-radiation equality. Here, $\rho_{\rm PBH,eq}$ is the energy density of PBHs at the epoch of matter-radiation equality. Multiplying dP_t/dt by the present average number density of PBHs, one can obtain the merger rate of PBH binaries as

$$R_{\rm PBH}(z) = \left(\frac{f_{\rm PBH}\Omega_{\rm CDM}\rho_{\rm c}}{M}\right)\frac{dP_t}{dt}. \tag{B2}$$

The redshift z is related to the cosmic time t through $t = \int_z^\infty dz'/[(1+z')H(z')]$, where $H(z) = H_0[\Omega_{r,0}(1+z)^4 + \Omega_{m,0}(1+z)^3 + \Omega_\Lambda]^{1/2}$ is the Hubble parameter at redshift z. The quantities $\Omega_{r,0}$ and $\Omega_{m,0}$ denote the present energy-density fractions of radiation and nonrelativistic matter, respectively. The present energy-density fraction of dark energy is derived as $\Omega_\Lambda = 1 - \Omega_{r,0} - \Omega_{m,0}$. Here, $\rho_{\rm c} = 3H_0^2 M_G^2$ is the critical energy density of the Universe. Throughout this paper, we adopt the ΛCDM model with cosmological parameters measured by the Planck satellite [128].

[8]As was discussed in the Introduction, here we use a monochromatic mass distribution of PBHs as a reasonable approximation. Therefore, we use the PBH abundance $f_{\rm PBH}$ instead of the PBH mass function $f(M)$.

APPENDIX C: ENERGY SPECTRUM OF GRAVITATIONAL WAVES

In the nonspinning limit, the inspiral-merger-ringdown energy spectrum for a BBH coalescence takes the following form [120,121]:

$$\frac{dE_{\rm GW}}{d\nu_{\rm s}}(\nu_{\rm s}) = \frac{(G\pi)^{2/3}M_c^{5/3}}{3} \times \begin{cases} \nu_{\rm s}^{-1/3} & \text{for } \nu_{\rm s} < \nu_1, \\ w_1\nu_{\rm s}^{2/3} & \text{for } \nu_1 \le \nu_{\rm s} < \nu_2, \\ w_2\frac{\sigma^4\nu_{\rm s}^2}{(\sigma^2+4(\nu_{\rm s}-\nu_2)^2)^2} & \text{for } \nu_2 \le \nu_{\rm s} \le \nu_3, \\ 0 & \text{for } \nu_3 < \nu_{\rm s}, \end{cases} \tag{C1}$$

where ν_s is the GW frequency in the source frame, and w_1 and w_2 are two normalization constants that make the spectrum continuous. The parameters ν_i $(i = 1, 2, 3)$ and σ can be expressed in terms of M_t and η as follows:

$$\pi M_t\nu_1 = (1 - 4.455 + 3.521) + 0.6437\eta - 0.05822\eta^2 - 7.092\eta^3, \tag{C2}$$

$$\pi M_t\nu_2 = (1 - 0.63)/2 + 0.1469\eta - 0.0249\eta^2 + 2.325\eta^3, \tag{C3}$$

$$\pi M_t\sigma = (1 - 0.63)/4 - 0.4098\eta + 1.829\eta^2 - 2.87\eta^3, \tag{C4}$$

$$\pi M_t\nu_3 = 0.3236 - 0.1331\eta - 0.2714\eta^2 + 4.922\eta^3, \tag{C5}$$

which can be found in Table I of Ref. [121]. Here, M_c is the chirp mass, i.e., $M_c^{5/3} = m_1m_2(m_1 + m_2)^{-1/3}$, and $M_t = m_1 + m_2$ is the total mass. The symmetric mass ratio is defined by $\eta = m_1m_2(m_1 + m_2)^{-2}$, which gives 0.25 in this work, since we assume a monochromatic mass for PBHs. The cutoff frequency is $\nu_{\rm cut} = \nu_3$.

APPENDIX D: CURVATURE-INDUCED GRAVITATIONAL WAVES IN A NUTSHELL

We briefly summarize the semianalytic calculation of the SGWB spectrum induced in the RD era from the nonlinear (tensor-scalar-scalar) mode coupling. The details are described in Ref. [76] and references therein. The energy-density fraction of the induced SGWB is given by

$$\Omega_{\rm GW}(k)|_{\rm today} = \frac{\Omega_{\rm r,0}}{24}\left(\frac{g_{*,\rho}(T)}{g_{*,\rho}(T_{\rm eq})}\right)\left(\frac{g_{*,s}(T)}{g_{*,s}(T_{\rm eq})}\right)^{-4/3} \times \left(\frac{k}{aH}\right)^2\overline{\mathrm{P}_h(\tau,k)}, \tag{D1}$$

where the cosmic temperature $T = T(M_H(k))$, the horizon mass $M_H(k)$, aH, and the conformal time τ are to be evaluated at (a time somewhat after) the horizon entry of the relevant mode (when $\Omega_{\rm GW}$ has reached a temporary asymptotic value). In fact, $T(M_H(k))$ can be numerically evaluated by combining Eq. (A6) with Eq. (A7). The last two factors in the above formula are given by

$$\left(\frac{k}{aH}\right)^2\overline{\mathrm{P}_h(\tau,k)} = 4\int_0^\infty dv \times \int_{-|1-v|}^{1+v} du\left[\frac{4v^2-(1+v^2-u^2)^2}{4uv}\right]^2 \times (k\tau)^2\overline{I^2(v,u,k\tau\gg1)}\mathcal{P}_\zeta(kv)\mathcal{P}_\zeta(ku). \tag{D2}$$

In the above equation, we have

$$(k\tau)^2\overline{I^2(v,u,k\tau\gg1)} = \frac{1}{2}\left(\frac{3(u^2+v^2-3)}{4u^3v^3}\right)^2\left(\left(-4uv+(u^2+v^2-3)\times\ln\left|\frac{3-(u+v)^2}{3-(u-v)^2}\right|\right)^2+\pi^2(u^2+v^2-3)^2\times\Theta(v+u-\sqrt{3})\right). \tag{D3}$$

Then, we combine the above three equations to compute the energy-density spectrum of the induced SGWB in this work. In the case of a delta-function source [Eq. (4)], the integral is easily calculated to obtain Eq. (11).

[1] B. P. Abbott *et al.* (Virgo and LIGO Scientific Collaborations), Phys. Rev. Lett. **116**, 061102 (2016).
[2] S. Hawking, Mon. Not. R. Astron. Soc. **152**, 75 (1971).
[3] B. J. Carr and S. W. Hawking, Mon. Not. R. Astron. Soc. **168**, 399 (1974).
[4] B. P. Abbott *et al.* (Virgo and LIGO Scientific Collaborations), Astrophys. J. **818**, L22 (2016).
[5] K. Belczynski, D. E. Holz, T. Bulik, and R. O'Shaughnessy, Nature (London) **534**, 512 (2016).
[6] M. C. Miller, Gen. Relativ. Gravit. **48**, 95 (2016).

[7] S. Bird, I. Cholis, J. B. Munoz, Y. Ali-Haimoud, M. Kamionkowski, E. D. Kovetz, A. Raccanelli, and A. G. Riess, Phys. Rev. Lett. **116**, 201301 (2016).
[8] M. Sasaki, T. Suyama, T. Tanaka, and S. Yokoyama, Phys. Rev. Lett. **117**, 061101 (2016).
[9] S. Clesse and J. Garca-Bellido, Phys. Dark Universe **10**, 002 (2016).
[10] Y. N. Eroshenko, J. Phys. Conf. Ser. **1051**, 012010 (2018).
[11] B. Carr, F. Kuhnel, and M. Sandstad, Phys. Rev. D **94**, 083504 (2016).
[12] A. Kashlinsky, Astrophys. J. **823**, L25 (2016).
[13] N. Bartolo *et al.*, J. Cosmol. Astropart. Phys. 12 (2016) 026.
[14] I. Cholis, J. Cosmol. Astropart. Phys. 06 (2017) 037.
[15] T. Harada, C.-M. Yoo, K. Kohri, K.-i. Nakao, and S. Jhingan, Astrophys. J. **833**, 61 (2016).
[16] J. Georg and S. Watson, J. High Energy Phys. 09 (2017) 138.
[17] T. Nakamura *et al.*, Prog. Theor. Exp. Phys. (**2016**), 093E01.
[18] A. Raccanelli, E. D. Kovetz, S. Bird, I. Cholis, and J. B. Munoz, Phys. Rev. D **94**, 023516 (2016).
[19] B. Carr, M. Raidal, T. Tenkanen, V. Vaskonen, and H. Veermäe, Phys. Rev. D **96**, 023514 (2017).
[20] M. Sasaki, T. Suyama, T. Tanaka, and S. Yokoyama, Classical Quantum Gravity **35**, 063001 (2018).
[21] G. Bertone and D. Hooper, Rev. Mod. Phys. **90**, 045002 (2018).
[22] A. Tan *et al.* (PandaX-II Collaboration), Phys. Rev. Lett. **117**, 121303 (2016).
[23] D. S. Akerib *et al.* (LUX Collaboration), Phys. Rev. Lett. **116**, 161301 (2016).
[24] L. Accardo *et al.* (AMS Collaboration), Phys. Rev. Lett. **113**, 121101 (2014).
[25] M. Ackermann *et al.* (Fermi-LAT Collaboration), Phys. Rev. Lett. **108**, 011103 (2012).
[26] B. J. Carr, K. Kohri, Y. Sendouda, and J. Yokoyama, Phys. Rev. D **81**, 104019 (2010).
[27] S. C. Novati, S. Mirzoyan, P. Jetzer, and G. Scarpetta, Mon. Not. R. Astron. Soc. **435**, 1582 (2013).
[28] E. Mediavilla, J. A. Munoz, E. Falco, V. Motta, E. Guerras, H. Canovas, C. Jean, A. Oscoz, and A. M. Mosquera, Astrophys. J. **706**, 1451 (2009).
[29] A. M. Green, Phys. Rev. D **94**, 063530 (2016).
[30] G. Chapline and P. H. Frampton, J. Cosmol. Astropart. Phys. 11 (2016) 042.
[31] L. Chen, Q.-G. Huang, and K. Wang, J. Cosmol. Astropart. Phys. 12 (2016) 044.
[32] Y. Ali-Haimoud and M. Kamionkowski, Phys. Rev. D **95**, 043534 (2017).
[33] V. Poulin, P. D. Serpico, F. Calore, S. Clesse, and K. Kohri, Phys. Rev. D **96**, 083524 (2017).
[34] K. Schutz and A. Liu, Phys. Rev. D **95**, 023002 (2017).
[35] B. P. Abbott *et al.* (LIGO Scientific and Virgo Collaborations), Phys. Rev. Lett. **121**, 231103 (2018).
[36] V. F. Mukhanov, H. A. Feldman, and R. H. Brandenberger, Phys. Rep. **215**, 203 (1992).
[37] C. E. Rhoades, Jr. and R. Ruffini, Phys. Rev. Lett. **32**, 324 (1974).
[38] B. J. Carr, arXiv:astro-ph/0511743.
[39] A. A. Starobinsky, JETP Lett. **30**, 682 (1979).
[40] A. A. Starobinsky, Phys. Lett. **91B**, 99 (1980).
[41] A. H. Guth, Phys. Rev. D **23**, 347 (1981).
[42] A. D. Linde, Phys. Lett. **108B**, 389 (1982).
[43] A. Albrecht and P. J. Steinhardt, Phys. Rev. Lett. **48**, 1220 (1982).
[44] K. Sato, Mon. Not. R. Astron. Soc. **195**, 467 (1981).
[45] A. D. Linde, Phys. Lett. **129B**, 177 (1983).
[46] K. Kohri, D. H. Lyth, and A. Melchiorri, J. Cosmol. Astropart. Phys. 04 (2008) 038.
[47] C. T. Byrnes, P. S. Cole, and S. P. Patil, arXiv:1811.11158.
[48] C.-M. Yoo, T. Harada, J. Garriga, and K. Kohri, Prog. Theor. Exp. Phys. **2018**, 123E01 (2018).
[49] B. P. Abbott *et al.* (Virgo, LIGO Scientific Collaboration), Phys. Rev. Lett. **118**, 121101 (2017).
[50] S. Wang, Y.-F. Wang, Q.-G. Huang, and T. G. F. Li, Phys. Rev. Lett. **120**, 191102 (2018).
[51] M. Raidal, V. Vaskonen, and H. Veerme, J. Cosmol. Astropart. Phys. 09 (2017) 037.
[52] V. Mandic, S. Bird, and I. Cholis, Phys. Rev. Lett. **117**, 201102 (2016).
[53] S. Clesse and J. Garca-Bellido, Phys. Dark Universe **18**, 105 (2017).
[54] S. Mollerach, D. Harari, and S. Matarrese, Phys. Rev. D **69**, 063002 (2004).
[55] K. N. Ananda, C. Clarkson, and D. Wands, Phys. Rev. D **75**, 123518 (2007).
[56] D. Baumann, P. J. Steinhardt, K. Takahashi, and K. Ichiki, Phys. Rev. D **76**, 084019 (2007).
[57] H. Assadullahi and D. Wands, Phys. Rev. D **81**, 023527 (2010).
[58] L. P. Grishchuk, Zh. Eksp. Teor. Fiz. **67**, 825 (1974); [Sov. Phys. JETP **40**, 409 (1975)].
[59] P. Creminelli, D. L. L. Nacir, M. Simonovic, G. Trevisan, and M. Zaldarriaga, J. Cosmol. Astropart. Phys. 11 (2015) 031.
[60] Q.-G. Huang, S. Wang, and W. Zhao, J. Cosmol. Astropart. Phys. 10 (2015) 035.
[61] Q.-G. Huang and S. Wang, Mon. Not. R. Astron. Soc. **483**, 2177 (2019).
[62] G. Cabass, L. Pagano, L. Salvati, M. Gerbino, E. Giusarma, and A. Melchiorri, Phys. Rev. D **93**, 063508 (2016).
[63] M. Escudero, H. Ramirez, L. Boubekeur, E. Giusarma, and O. Mena, J. Cosmol. Astropart. Phys. 02 (2016) 020.
[64] J. Errard, S. M. Feeney, H. V. Peiris, and A. H. Jaffe, J. Cosmol. Astropart. Phys. 03 (2016) 052.
[65] M. Kamionkowski and E. D. Kovetz, Annu. Rev. Astron. Astrophys. **54**, 227 (2016).
[66] L. Santos, K. Wang, and W. Zhao, J. Cosmol. Astropart. Phys. 07 (2016) 029.
[67] M. C. Guzzetti, N. Bartolo, M. Liguori, and S. Matarrese, Riv. Nuovo Cimento **39**, 399 (2016).
[68] P. D. Lasky *et al.*, Phys. Rev. X **6**, 011035 (2016).
[69] E. Bugaev and P. Klimai, Phys. Rev. D **81**, 023517 (2010).
[70] L. Alabidi, K. Kohri, M. Sasaki, and Y. Sendouda, J. Cosmol. Astropart. Phys. 09 (2012) 017.

[71] H. Assadullahi and D. Wands, Phys. Rev. D **79**, 083511 (2009).
[72] L. Alabidi, K. Kohri, M. Sasaki, and Y. Sendouda, J. Cosmol. Astropart. Phys. 05 (2013) 033.
[73] R.-G. Cai, S. Pi, S.-J. Wang, and X.-Y. Yang J. Cosmol. Astropart. Phys. 05 (2019) 013.
[74] R.-G. Cai, S. Pi, and M. Sasaki, arXiv:1810.11000.
[75] C. Unal, Phys. Rev. D **99**, 041301 (2019).
[76] K. Kohri and T. Terada, Phys. Rev. D **97**, 123532 (2018).
[77] J. R. Espinosa, D. Racco, and A. Riotto, J. Cosmol. Astropart. Phys. 09 (2018) 012.
[78] K. Inomata, M. Kawasaki, K. Mukaida, Y. Tada, and T. T. Yanagida, Phys. Rev. D **95**, 123510 (2017).
[79] K. Inomata and T. Nakama, Phys. Rev. D **99**, 043511 (2019).
[80] N. Orlofsky, A. Pierce, and J. D. Wells, Phys. Rev. D **95**, 063518 (2017).
[81] E. Bugaev and P. Klimai, Phys. Rev. D **83**, 083521 (2011).
[82] R. Saito and J. Yokoyama, Phys. Rev. Lett. **102**, 161101 (2009); **107**, 069901(E) (2011).
[83] R. Saito and J. Yokoyama, Prog. Theor. Phys. **123**, 867 (2010); **126**, 351(E) (2011).
[84] T. Nakama and T. Suyama, Phys. Rev. D **94**, 043507 (2016).
[85] M. Pitkin, S. Reid, S. Rowan, and J. Hough, Living Rev. Relativity **14**, 5 (2011).
[86] C. J. Moore, R. H. Cole, and C. P. L. Berry, Classical Quantum Gravity **32**, 015014 (2015); Proc. Sci. MRU020 (2007).
[87] H. Audley *et al.* (LISA Collaboration), arXiv:1702.00786.
[88] T. Robson, J. N. Cornish, and C. Liug, Classical Quantum Gravity **36**, 105011 (2019).
[89] S. Sato *et al.*, J. Phys. Conf. Ser. **840**, 012010 (2017).
[90] S. Isoyama, H. Nakano, and T. Nakamura, Prog. Theor. Exp. Phys. **2018**, 073E01 (2018).
[91] G. M. Harry, P. Fritschel, D. A. Shaddock, W. Folkner, and E. S. Phinney, Classical Quantum Gravity **23**, 4887 (2006); **23**, 7361(E) (2006).
[92] M. Punturo *et al.*, Classical Quantum Gravity **27**, 194002 (2010).
[93] B. P. Abbott *et al.* (Virgo and LIGO Scientific Collaborations), Phys. Rev. Lett. **116**, 131102 (2016).
[94] N. Bartolo, V. De Luca, G. Franciolini, M. Peloso, and A. Riotto, arXiv:1810.12218.
[95] N. Bartolo, V. De Luca, G. Franciolini, M. Peloso, D. Racco, and A. Riotto, arXiv:1810.12224.
[96] S. Clesse, J. García-Bellido, and S. Orani, arXiv: 1812.11011.
[97] K. Saikawa and S. Shirai, J. Cosmol. Astropart. Phys. 05 (2018) 035.
[98] J. Yokoyama, Phys. Rev. D **58**, 107502 (1998).
[99] T. Harada, C.-M. Yoo, and K. Kohri, Phys. Rev. D **88**, 084051 (2013); **89**, 029903(E) (2014).
[100] T. Harada, C.-M. Yoo, T. Nakama, and Y. Koga, Phys. Rev. D **91**, 084057 (2015).
[101] S. Young, C. T. Byrnes, and M. Sasaki, J. Cosmol. Astropart. Phys. 07 (2014) 045.
[102] K. Ando, K. Inomata, and M. Kawasaki, Phys. Rev. D **97**, 103528 (2018).
[103] W. H. Press and P. Schechter, Astrophys. J. **187**, 425 (1974).
[104] J. C. Niemeyer and K. Jedamzik, Phys. Rev. Lett. **80**, 5481 (1998).
[105] H. Niikura *et al.*, arXiv:1701.02151.
[106] H. Niikura, M. Takada, S. Yokoyama, T. Sumi, and S. Masaki, Phys. Rev. D **99**, 083503 (2019).
[107] P. Tisserand *et al.* (EROS-2 Collaboration), Astron. Astrophys. **469**, 387 (2007).
[108] R. A. Allsman *et al.* (Macho Collaboration), Astrophys. J. **550**, L169 (2001).
[109] M. Oguri, J. M. Diego, N. Kaiser, P. L. Kelly, and T. Broadhurst, Phys. Rev. D **97**, 023518 (2018).
[110] T. Nakamura, M. Sasaki, T. Tanaka, and K. S. Thorne, Astrophys. J. **487**, L139 (1997).
[111] K. Ioka, T. Chiba, T. Tanaka, and T. Nakamura, Phys. Rev. D **58**, 063003 (1998).
[112] Y. Ali-Haimoud, E. D. Kovetz, and M. Kamionkowski, Phys. Rev. D **96**, 123523 (2017).
[113] K. Hayasaki, K. Takahashi, Y. Sendouda, and S. Nagataki, Publ. Astron. Soc. Jpn. **68**, 66 (2016).
[114] G. Ballesteros, P. D. Serpico, and M. Taoso, J. Cosmol. Astropart. Phys. 10 (2018) 043.
[115] Z.-C. Chen and Q.-G. Huang, Astrophys. J. **864**, 61 (2018),
[116] M. Raidal, C. Spethmann, V. Vaskonen, and H. Veermäe, J. Cosmol. Astropart. Phys. 02 (2019) 018.
[117] L. Liu, Z.-K. Guo, and R.-G. Cai, Phys. Rev. D **99**, 063523 (2019).
[118] R. Magee, A.-S. Deutsch, P. McClincy, C. Hanna, C. Horst, D. Meacher, C. Messick, S. Shandera, and M. Wade, Phys. Rev. D **98**, 103024 (2018).
[119] B. Allen and J. D. Romano, Phys. Rev. D **59**, 102001 (1999).
[120] P. Ajith, S. Babak, Y. Chen, M. Hewitson, B. Krishnan, A. M. Sintes, J. T. Whelan, B. Brügmann, P. Diener, N. Dorband *et al.*, Phys. Rev. D **77**, 104017 (2008).
[121] P. Ajith, M. Hannam, S. Husa, Y. Chen, B. Brügmann, N. Dorband, D. Müller, F. Ohme, D. Pollney, C. Reisswig *et al.*, Phys. Rev. Lett. **106**, 241101 (2011).
[122] C. J. Moore, R. H. Cole, and C. P. L. Berry, Classical Quantum Gravity **32**, 015014 (2015).
[123] Y. Kikuta, K. Kohri, and E. So, arXiv:1405.4166.
[124] M. Kawasaki and H. Nakatsuka, arXiv:1903.02994.
[125] V. De Luca, G. Franciolini, A. Kehagias, M. Peloso, A. Riotto, and C. Unal, arXiv:1904.00970.
[126] S. Young, I. Musco, and C. T. Byrnes, arXiv:1904.00984.
[127] J. Garcia-Bellido, M. Peloso, and C. Unal, J. Cosmol. Astropart. Phys. 09 (2017) 013.
[128] P. A. R. Ade *et al.* (Planck Collaboration), Astron. Astrophys. **594**, A13 (2016).

Correction: The previously published Figures 1–7 and related text contained incorrect information for sensitivity values and have been replaced.